Dynamical neutron diffraction in a thick-crystal interferometer

J. Arthur,* C. G. Shull, and A. Zeilinger†
Massachusetts Institute of Technology, Cambridge, Massachusetts 02139
(Received 7 June 1985)

The Massachusetts Institute of Technology (MIT) neutron interferometer consisting of two thick perfect-crystal plates of silicon is described, its operation is analyzed within the framework of dynamical diffraction theory, and experimental results illustrating some aspects of its operation are presented. It is found theoretically that the details of the distribution of intensity in the neutron beams leaving the device and the changes in the intensity distribution induced by phase-shifting elements placed between the crystals depend sensitively on the coherence properties of the neutron radiation as it enters the interferometer. A slit placed in front of the first crystal plate will modify the incident-beam coherence properties enough to affect the interferometer operation, if the width of the slit is comparable to or smaller than the *Pendellösung* length which characterizes the dynamical diffraction in the crystal plates. High-resolution scans of the intensity distribution of the neutron radiation leaving the interferometer were performed while the incident beam was defined by a wide slit (approximately 1 mm in width) or alternatively a narrow slit (approximately 0.1 mm in width, comparable to the *Pendellösung* length), with phase-shifting devices placed between the crystals. The data agree closely with the theoretical calculations, and demonstrate the spatially extended coherence properties of a neutron wave traversing such an interferometer.

I. INTRODUCTION

The observation by Sippel *et al.*[1] and the detailed study by Shull[2] of *Pendellösung* structure in neutron radiation diffracted from single thick perfect silicon crystals in Laue geometry were the first clear demonstrations that extended spatial coherence can be induced in a neutron wave function by crystal diffraction. A symmetric arrangement of two identical thick perfect crystals provides an even more dramatic display of neutron wave coherence effects. This paper presents an analysis of such a two-crystal Laue-case neutron interferometer, along with experimental data illustrating its operation. In contrast to three-crystal interferometer systems of the Bonse-Hart type,[3] the operation of a two-crystal system depends critically on dynamical diffraction effects inside the crystals, such as Borrmann fan spreading. Therefore, subtle dynamical effects are more readily apparent in observations with a two-crystal interferometer. This is true for a two-crystal Bragg-case interferometer,[4] as well as for the Laue-case interferometer considered here.

Dynamical diffraction theory is used to analyze the wave function of a neutron beam diffracting in a perfect crystal. There are several good presentations of the dynamical theory of neutron diffraction[5–7] and the closely related theory for x rays.[8,9] The coherence effects described in the present paper are greatly influenced by the boundary conditions imposed on the incident beam. Therefore, many references will be made to Ref. 7, where the boundary-value problem is stressed. The notation used here is that of the review paper by Rauch and Petrascheck.[5] Three operational configurations of the two-crystal interferometer are considered. In the first, the incident beam is defined by a slit much wider than the *Pendellösung* length, which is the characteristic length in dynamical diffraction. In this case, to a very good approximation, the response to a perturbation of the phase of the diffracting radiation appears as an intensity change in an exit beam whose spatial structure is unchanged by the perturbation. A contrasting configuration, in which the incident beam is constrained by a slit much narrower than the *Pendellösung* length, produces an exit beam with much more complicated spatial structure. Both structure and intensity are modified by phase perturbations. A third configuration, which is more easily accessible experimentally than the second one, uses an incident beam defined by a slit of width about equal to the *Pendellösung* length, and still exhibits interesting spatial structure effects.

II. DESCRIPTION OF THE MIT TWO-CRYSTAL INTERFEROMETER

Figure 1 shows a perspective view and a schematic top view of the two-crystal interferometer at the Massachusetts Institute of Technology (MIT) Neutron Diffraction Laboratory. It was constructed in 1978 by A. Zeilinger and C. G. Shull, and an account of early experiments performed with it is given by Zeilinger *et al.*[10] Some similar devices have been used by Kikuta.[11] Its principal features are two identical crystal plates (or "ears") which project from, but remain attached to, a base, the entire assembly having been cut from a single-crystal ingot of very pure silicon. The ear thicknesses are identical to within 3 μm, and they are oriented for symmetric Laue diffraction of 1.564 Å neutrons from the (400) crystal planes. The base serves to precisely maintain the relative orientation of the two ears (the failure of an attempt by Shull in 1968 to observe interference action in a system of two separated crystals is believed to have been

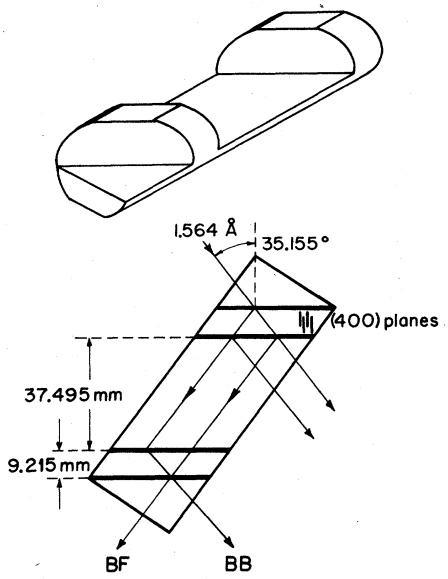

FIG. 1. Illustration of the MIT two-crystal interferometer, cut from a single perfect crystal of silicon.

due to alignment problems).

In operation, the interferometer rests on its base in an environment carefully designed to eliminate harmful vibrations and to reduce temperature drifts to <5 mdeg/day.[12] A collimated, semimonochromatic beam of neutrons passes into the first crystal ear through an entrance slit opening whose width can be adjusted. Exit radiation from the back face of the second crystal ear can be scanned with an exit slit, also adjustable, and final detection is performed in either or both of the indicated emerging beams by proportional gas counters. Various operational test devices such as slit openings, phase step plates, and phase gradient wedges may be placed in the beam between the two crystals without harmful contact with the interferometer.

III. WIDE-BEAM RAY OPTICS

A. Wave functions and flux propagation directions

The interferometer is most frequently used with a neutron beam prepared by an entrance slit that is approximately 1 mm wide. This is much wider than the *Pendellösung* length, which is defined by

$$\Delta=\frac{2\pi\cos\theta}{k}\frac{E}{V_G}e^{+W},$$

where θ is the Bragg angle, k is the magnitude of the incident wave vector, E is the incident neutron kinetic energy, V_G is the Fourier component of the neutron-crystal interaction potential associated with the chosen Bragg reflection, and $\exp(W)$ is the inverse Debye-Waller amplitude factor. For the conditions of operation of the MIT interferometer, $\Delta=8.41\times10^{-2}$ mm.

The incident beam, generated in a sizable volume of space in the reactor interior by random events, and prepared by large slits and a mosaic monochromator crystal, can best be described as having no consistent coherence properties among different momentum components on a scale relevant to the dynamical diffraction effects considered in the present paper. The incident beam can, therefore, be treated as an incoherent mixture of plane waves, with a distribution of wavelengths and propagation directions.

A single plane wave falling on a perfect crystal in symmetric Laue orientation excites an amplitude at a point $\mathbf{r}=(x,z)$ in the crystal that can be expressed as[5,7]

$$\psi(\mathbf{r})=\exp\left[i\mathbf{K}_0\cdot\mathbf{r}-i\frac{\pi}{\Delta}\frac{x}{\tan\theta}y\right]\left[\cos\left[\frac{\pi}{\Delta}z(y^2+1)^{1/2}\right]+\frac{iy}{(y^2+1)^{1/2}}\sin\left[\frac{\pi}{\Delta}z(y^2+1)^{1/2}\right]\right]$$
$$+\exp\left[i(\mathbf{K}_0+\mathbf{G})\cdot\mathbf{r}-i\frac{\pi}{\Delta}\frac{x}{\tan\theta}y\right]\left[-i\frac{1}{(y^2+1)^{1/2}}\sin\left[\frac{\pi}{\Delta}z(y^2+1)^{1/2}\right]\right], \quad (1)$$

where $\mathbf{K}_0$ is a wave vector which exactly satisfies Bragg's law for a neutron wave inside the average potential of the crystalline medium, and y is a dimensionless parameter related to the deviation of the incident wave propagation direction θ_i from the Bragg angle θ by

$$y=\frac{2\Delta\sin\theta}{\lambda}(\theta-\theta_i). \quad (2)$$

The wave amplitude given by Eq. (1) actually represents a superposition of two solutions to the Schrödinger equation in the crystal that are both excited by the same incident wave. Each of these solutions has the form of a plane wave propagating in the general direction of $\mathbf{K}_0$ (the forward direction) plus another plane wave propagating in the Bragg-reflected direction of $(\mathbf{K}_0+\mathbf{G})$. Note that $|\mathbf{K}_0|\gg\pi/\Delta$. The corresponding waves of the two solutions have wave vectors with slightly different magnitudes, and their interference gives rise to the sine and cosine factors (the *Pendellösung* phenomenon).

The use of plane-wave solutions to describe waves that are spatially limited by an entrance slit and, thus, not strictly planar is analogous to the use of light ray paths in the analysis of optical systems. The ray approach is valid so long as the diffraction effects arising from the spatial limitation of the waves do not cause appreciable spreading of the ray as it traverses the system. A neutron ray dif-

fracting through a perfect crystal will maintain its ray quality if its spatial limitation is much wider than the *Pendellösung* length.[7]

It can be shown[5] that the probability flux associated with each of the solutions depends on y in the following manner: One solution, often referred to as the "α" solution, produces a flux that penetrates into the crystal at an angle Ω with respect to the crystal planes that is given by (see Fig. 2)

$$\tan\Omega = \frac{-y}{(y^2+1)^{1/2}}\tan\theta \ . \tag{3a}$$

The other solution, known as the "β" solution, produces a flux that moves through the crystal at an angle Ω', where

$$\tan\Omega' = \frac{+y}{(y^2+1)^{1/2}}\tan\theta \ . \tag{3b}$$

When the first crystal of the interferometer is illuminated by a single plane wave through a 1-mm entrance slit, the overlapping waves described by Eq. (1) are produced together just below the surface of the illuminated region of the crystal, but as they flow deeper into the crystal they become spatially separated.

When the two rays reach the back face of the first crystal, each ray separates into a wave traveling approximately in the direction of $\mathbf{K}_0$ and another traveling approximately in the direction of $(\mathbf{K}_0+\mathbf{G})$. In the MIT interferometer, the forward-diffracted ($\mathbf{K}_0$) rays are discarded, but the reflected $(\mathbf{K}_0+\mathbf{G})$ rays fall on the second interferometer crystal. Since this crystal is identical to and oriented in exactly the same way as the first crystal, the rays generated in it are similar to those generated in the first crystal. Two of these four rays overlap as they reach the back face of the second crystal, and all four rays generate forward and reflected rays behind the crystal. It is now apparent why this two-crystal device is called an interferometer: it causes an incident wave to be coherently split into several spatially separated waves, and then brings two of the separated waves back into coherent superposition. Perturbations of the relative phases of the separated rays between the crystals will cause interference action in the overlapping rays leaving the second crystal.

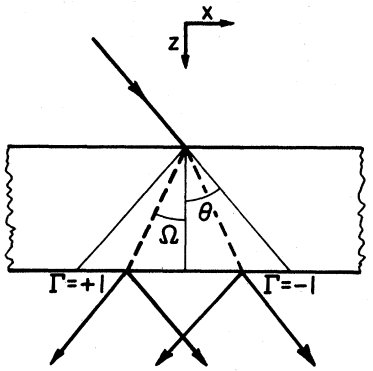

FIG. 2. Path of a typical very-well-collimated, monochromatic neutron ray diffracting in a thick perfect crystal. The coordinate systems (x,z) and (Γ,z) are indicated. $\Gamma=\tan\Omega/\tan\theta$.

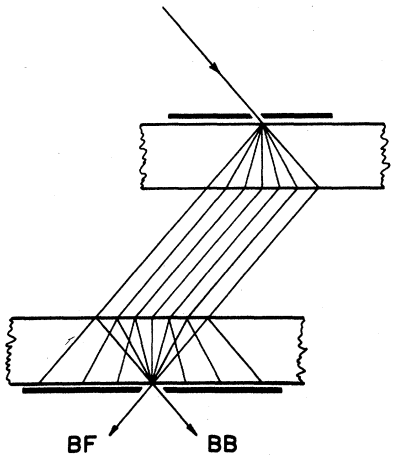

FIG. 3. Ray paths in the two-crystal interferometer illuminated by a divergent incident beam through a wide entrance slit, illustrating the recombination point at the back face of the second crystal. Coherence exists between rays symmetrically located about the center of the wide beam between the crystals.

It is also clear that the interference action appears only in the superimposed rays, and not in the other radiation leaving the second crystal. Figure 3 illustrates the response of the interferometer to a collection of incident rays with different values of the parameter y, as would be found in a real experiment. The entire region defined by the Borrmann fan in the first crystal contains radiation, but, with a wide entrance slit, coherence exists only between rays symmetrically located about the center of this region. All of the pairs of coherently superimposed rays exit the second cyrstal at the same "focal spot," causing a central peak in the distribution of intensity observed leaving the crystal in either the forward or reflected direction. The intensity of this central peak contains all of the interferometer action, and the other radiation leaving the interferometer is normally blocked by an exit slit of about the same width as the entrance slit in front of the first crystal.

B. The action of a phase wedge

The utility of this neutron interferometer lies in its ability to sense the phase effects of very weak perturbations of the neutron waves between the crystals.[13–15] Only one phase-shifting technique will be discussed here, to demonstrate the influence of the preparation of the incident wave on the interferometer performance. This technique involves shifting the phase of each ray between the crystals by an amount proportional to the ray's x coordinate. A wedge of a pure, homogeneous material such as aluminum or silicon is inserted between the interferometer crystals so that the different rays pass through different thicknesses of material. Since the neutron index of refraction of the material differs slightly from that of air, to a very good approximation the wedge simply induces a relative phase shift in each ray proportional to the ray's position. A convenient coordinate for measuring the position of a ray is Γ, defined within the first crystal by

$$\Gamma=\frac{-x}{z\tan\theta}=\frac{\tan\Omega}{\tan\theta}\ . \tag{4a}$$

Equations (3) show that the neutron rays in the first crystal follow lines of constant Γ (see Fig. 2). The values of Γ found along the back face of the first crystal can be used to locate rays traveling in space between the two crystals. Along the back face of the second crystal an analogous coordinate $\hat{\Gamma}$ can be defined as

$$\hat{\Gamma}=\frac{+(x-x_0)}{(z-z_0)\tan\theta}\ , \tag{4b}$$

where (x_0,z_0) is the midpoint of the neutron beam striking the front face of this crystal, and the sign convention emphasizes the fact that the scattering vector in the second crystal is reversed with respect to that in the first crystal. (The reason for extending the Γ-coordinate system to the second crystal in this fashion will become clear later, when the operation of the interferometer with a very small entrance slit is considered.) The rays traversing the interferometer lie between $\Gamma=+1$ and $\Gamma=-1$ in the first crystal and in the space between the crystals. At the back face of the second crystal, some rays can be found throughout the range $\hat{\Gamma}=-2$ to $\hat{\Gamma}=+2$, but half of the rays are superimposed at $\hat{\Gamma}=0$.

The intensities of the beams emanating from the focal spot on the second crystal, referred to as the BB (for "Bragg-Bragg") beam and the BF ("Bragg-Forward") beam, can be calculated starting with the wave functions given by Eq. (1). It is found that the two rays excited by each incident plane wave which recombine at the focal spot are in (out of) phase as they recombine to form the BB (BF) exit beam, in the absence of external perturbations. The amplitude contributed by each of these rays to the BB exit beam is $[-\frac{1}{4}(1-\Gamma^2)]$, where $\pm\Gamma$ give the positions of the rays in the region between the interferometer crystals. The amplitudes contributed to the BF beam are

$$[\pm\tfrac{1}{4}(1-\Gamma^2)^{1/2}(1-\Gamma)]\ ,$$

where the two recombining rays take opposite signs. The factor of $\frac{1}{4}$ merely indicates that each ray has been split twice, in the first crystal and in the second. Summing the intensities due to the coherent combinations of the interfering ray pairs (including the effects of external phase perturbations) gives the exit beam intensities. The sum over rays is converted to an integral over Γ using the density of rays in the interferometer as a function of Γ, which is found using Eqs. (3) and the assumption that the plane waves incident on the entrance slit are characterized by a uniform distribution over all values of the parameter y. This latter approximation is valid because y is such a very sensitive measure of the propagation directions of the incident waves and because the angular divergence of the incident radiation is very much greater than the angular acceptance of the crystal. The density function is

$$D(\Gamma)d\Gamma=I_0\,|\,dy\,|=I_0\frac{1}{(1-\Gamma^2)^{3/2}}d\Gamma\ . \tag{5}$$

With a phase-shifting wedge between the interferometer crystals, the BB beam intensity is

$$I_{\rm BB}=\int_{-1}^{1}d\Gamma\left|-\tfrac{1}{4}(1-\Gamma^2)e^{i\phi_0\Gamma}-\tfrac{1}{4}(1-\Gamma^2)e^{-i\phi_0\Gamma}\right|^2\frac{I_0}{(1-\Gamma^2)^{3/2}}$$
$$=I_0\frac{\pi}{16}+I_0\frac{\pi}{8}\frac{J_1(2\phi_0)}{2\phi_0}\ , \tag{6a}$$

and the BF beam intensity is

$$I_{\rm BF}=\int_{-1}^{1}d\Gamma\left|\tfrac{1}{4}(1-\Gamma^2)^{1/2}(1-\Gamma)e^{i\phi_0\Gamma}-\tfrac{1}{4}(1-\Gamma^2)^{1/2}(1+\Gamma)e^{-i\phi_0\Gamma}\right|^2\frac{I_0}{(1-\Gamma^2)^{3/2}}$$
$$=I_0\frac{3\pi}{16}-I_0\frac{\pi}{8}\frac{J_1(2\phi_0)}{2\phi_0}\ . \tag{6b}$$

The parameter ϕ_0 is related to the average scattering length and density of the wedge material, to the wedge apex angle, and to the neutron wavelength. The phase difference between the coherent rays propagating at the edges of the beam between the interferometer crystals ($\Gamma=+1$ and $\Gamma=-1$) is equal to $2\phi_0$. Note that the sum of the BB and BF intensities is independent of ϕ_0; neutrons cannot be created or destroyed by a perturbation of their phases.

C. Wide-slit experiments

Figure 4 shows the measured BB beam intensity as a function of $2\phi_0$, along with the calculated curve. Three fitting parameters were used to adjust the curve to the data. Two of these simply set the maximum intensity and the background level. The third reveals a peculiar aspect of the performance of the MIT interferometer: the device exhibits an intrinsic phase wedge effect, as if a wedge characterized by $2\phi_0\approx 8$ rad were permanently mounted between the crystals. The maximum BB intensity shown in Fig. 4 was achieved when the external wedge just can-

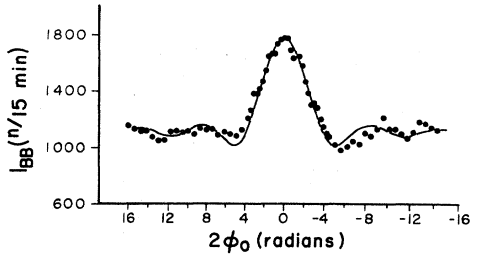

FIG. 4. Measured and theoretical response of the BB central peak intensity to a linear phase shifter (adjustable phase wedge), using wide ($\sim$1 mm) slits. $2\phi_0$ is the phase difference between the extreme ($\Gamma=\pm1$) rays. The action of the wedge can be viewed as a refractive bending of the neutron beam, giving an angular FWHM for the central peak of 2.47×10^{-3} seconds of arc.

celed this intrinsic effect. The reason for this behavior is still not well understood. There are external, environmental effects which can cause phase perturbations similar to those induced by a wedge.[15] However, the one observed seems to be a property of the interferometer crystal rather than its environment, since the intrinsic effect changes sign when the interferometer is turned around so that the first ear becomes the second ear and vice versa. Also, the intrinsic wedge action is not uniform over the entire interferometer. Experiments using vertically restricted neutron beams have shown that the effect is somewhat more pronounced near the top edges of the ears, and less pronounced near the connecting base. It is plausible that the effect is caused by small permanent strains induced in the crystal during its growth or cutting, but the true cause has not been determined. In Fig. 4 the abscissa values give the effective phase wedge parameter, corrected for the intrinsic wedge contribution.

It may be noted that the action of a phase wedge can be interpreted as a refractive bending of the neutron beam, producing an effective rotation of the second interferometer crystal with respect to the first. With this interpretation, the peak in Fig. 4 can be viewed as a rocking curve with a full width at half maximum (FWHM) of only 2.47×10^{-3} seconds of arc. Such extremely high angular resolution is characteristic of double-perfect-crystal Laue-case rocking curves.[16]

The action of the two-crystal interferometer with a wide entrance slit can be summed up in the following manner. A plane wave incident on the wide entrance slit produces a neutron ray. This ray is coherently split by diffraction in the first crystal so that two parallel, coherent rays travel between the two crystals, and these rays are partially recombined by diffraction in the second crystal. The ray paths within the interferometer depend very sensitively on the direction of propagation of the incident plane wave, but the recombination spot is always the same. The interference between the coherently recombined rays determines the distribution of intensity between the BB and BF beams leaving the recombination spot, but there is no fine structure to these beams. It will next be shown that the interferometer action manifests itself somewhat differently when the entrance slit is very narrow.

IV. THE VERY-NARROW-BEAM CASE

A. Theoretical considerations

An entrance slit with width much less than the *Pendellösung* length modifies an incident plane wave through single-slit diffraction to such an extent that its crystal diffraction characteristics are not at all plane wavelike (even though the *Pendellösung* length is about 5 orders of magnitude larger than the neutron wavelength so that such a slit is still immense on a neutron wavelength scale). The wave amplitude generated in the first interferometer crystal by such a wave can be found by taking a superposition of plane-wave solutions of the form given by Eq. (1) or by directly solving the dynamical diffraction problem with a spatially very limited incident wave. Using the (Γ,z) coordinate system, the neutron wave amplitude excited at a point (Γ,z) in the crystal by a wave incident through a very narrow slit on the crystal surface at (0,0) can be written[7]

$$\psi(\Gamma,z)=e^{i\mathbf{K}_0\cdot\mathbf{r}}\left[\frac{-\pi z}{2\Delta}\left(\frac{1-\Gamma}{1+\Gamma}\right)^{1/2}J_1((\pi z/\Delta)(1-\Gamma^2)^{1/2})[\Theta(1-\Gamma)-\Theta(-1-\Gamma)]+\delta(1+\Gamma)\right]$$
$$+e^{i(\mathbf{K}_0+\mathbf{G})\cdot\mathbf{r}}\left[-i\frac{\pi z}{2\Delta}J_0((\pi z/\Delta)(1-\Gamma^2)^{1/2})[\Theta(1-\Gamma)-\Theta(-1-\Gamma)]\right], \tag{7}$$

where $\mathbf{r}$ is the vector from (0,0) to (Γ,z), and J_1 and J_0 are ordinary Bessel functions. Note that this wave amplitude does not depend on the initial characteristics of the incident wave in front of the entrance slit, and that the unit step functions Θ limit the nonzero part of this wave to the triangular region of crystal where $-1<\Gamma<1$.

The concept of a neutron ray is not useful in this situation. An initially very localized wave (at the entrance slit) spreads out to fill the entire Borrmann fan in the first interferometer crystal, and this spread-out wave possesses spatial structure on a *Pendellösung*-length scale, described by Bessel functions. At the back face of the crystal, the wave separates into a wide, spatially modulated wave moving approximately in the direction of $\mathbf{K}_0$ and another large modulated wave moving approximately in the direction of $(\mathbf{K}_0+\mathbf{G})$. The scale of the modulation is Δ, 5 orders of magnitude greater than the neutron wavelength, so the modulated structure of these waves remains essentially unchanged as they propagate through free space behind the first crystal. In the MIT interferometer, the wave moving in the $(\mathbf{K}_0+\mathbf{G})$ direction falls on the second interferometer crystal. Each point on the surface of this crystal, illuminated by this large, modulated, but coherent wave, generates a diffracted wave similar to the one given by Eq. (7). The net wave is found by coherently summing the individual wavelets generated by all the illuminated points, taking into account their relative phases and amplitudes. Upon careful consideration of the phase at each surface point, including the realization that the crystal surface consists of a discrete lattice of atoms, it is found that the wave amplitude generated in the second crystal can be written as a convolution of Bessel functions, multi-

plied by an overall phase factor. At the back face of the second crystal, this complicated wave generates waves leaving the crystal in the directions of $\mathbf{K}_0$ and $(\mathbf{K}_0+\mathbf{G})$. Only the wave that has been Bragg reflected in both the first and second crystals will be considered in detail here because, for reasons related to geometry and background counting rates, this BB wave is much easier to study experimentally. If the thickness of each crystal is t and if the effective neutron source on the first crystal surface is at (0,0), the BB wave amplitude behind the second crystal as a function of $\hat{\Gamma}$ [recall Eqs. (4) and Fig. 3] can be written

$$\psi_{\mathrm{BB}}(\hat{\Gamma})=\text{const}\times\int_{\max(-1-\hat{\Gamma},\,-1)}^{\min(1-\hat{\Gamma},\,1)} d\Gamma\, J_0((\pi t/\Delta)[1-(\hat{\Gamma}+\Gamma)^2]^{1/2})J_0((\pi t/\Delta)(1-\Gamma^2)^{1/2})\ . \tag{8}$$

The limits on the convolution integral are due to the step-function factors in Eq. (7). [The value of $\min(1-\hat{\Gamma},1)$ is equal to the smaller of the two quantities, while the value of $\max(-1-\hat{\Gamma},-1)$ is equal to the greater of the two.] They have the effect of limiting the wave function to the region $-2<\hat{\Gamma}<2$.

The factor $\pi t/\Delta$ appearing in the arguments of the Bessel functions in Eq. (8) has a value, for the MIT interferometer, of 344. Thus, the Bessel functions are highly oscillatory functions of Γ. This means that the value of the convolution integral is quite small, because of cancellation effects, except when $\hat{\Gamma}$ is near zero. In other words, the intensity of the BB radiation possesses a sharp peak at $\hat{\Gamma}=0$. This is reminiscent of the central peak in the BB intensity observed using a wide entrance slit. However, in the very-small-slit case the radiation in the region between the interferometer crystals is coherent across the entire Borrmann fan, and phase perturbations lead to dramatic changes in the BB intensity distribution. Consider the placement of a phase wedge between the crystals. The linear phase shifts introduced modify Eq. (8) slightly, so that the BB intensity distribution becomes

$$I_{\mathrm{BB}}(\hat{\Gamma})=\text{const}\times\left|\int_{\max(-1-\hat{\Gamma},\,-1)}^{\min(1-\hat{\Gamma},\,1)} d\Gamma\, J_0((\pi t/\Delta)[1-(\hat{\Gamma}+\Gamma)^2]^{1/2})J_0((\pi t/\Delta)(1-\Gamma^2)^{1/2})e^{i\phi_0\Gamma}\right|^2 . \tag{9}$$

Figure 5 shows numerical calculations of I_{BB} for different values of $\hat{\Gamma}$ and wedge parameter, based on Eq. (9). The intensity at points away from $\hat{\Gamma}=0$ is affected in a pronounced way with increasing structure and splitting as the wedge action is increased. The intensity at points outside the small $\hat{\Gamma}$ range shown in Fig. 5 continues to oscillate with a period comparable to the period of the oscillations in Fig. 5, but with an amplitude that is only about $\Delta/\pi t=1/344$ times as large as the large peaks.

Within the ray optics model, it might also be expected that refractive bending of the rays would cause a change in the intensity distribution at the exit surface of the second crystal. However, the ray optics model does not allow for interference action between rays at any point other than $\hat{\Gamma}=0$, and this model cannot produce the complicated intensity patterns of Fig. 5. The ray model fails because diffraction effects at the small entrance slit make it impossible to define ray paths within the crystals.

B. Relationships between the narrow-slit case and the wide-slit case

Having stressed the differences in the operation of the interferometer with wide and with very narrow entrance slits, it is now appropriate to present some fundamental relationships between these cases. First, consider again the way in which the neutron ray optics treatment of the wide-slit case was derived from the dynamical diffraction theory of plane incident waves. The neutron rays which combine at the focus spot on the back face of the second crystal contribute amplitudes and phases that are very similar to the amplitudes and phases that would be present at the same spot if there were no entrance slit, and plane waves illuminated the entire front face of the first crystal. Therefore, it is instructive to consider the case of no entrance slit.[19]

The performance of the interferometer with full-plane-wave illumination can be easily deduced from Eq. (1). A single plane wave, diffracted twice, produces a BB wave with intensity equal to

$$\left|\frac{\sin[(\pi t/\Delta)(y^2+1)^{1/2}]}{(y^2+1)^{1/2}}\right|^2\left|\frac{\sin[(\pi t/\Delta)(y^2+1)^{1/2}]}{(y^2+1)^{1/2}}\right|^2 .$$

The BB intensity due to a mixture of incident plane waves is given by an integral over the parameter y. Now, if a wedge is inserted between the interferometer crystals, each

of the plane waves will be deflected slightly by the prism action, so the value of y for each wave will be changed by a small amount δy. To a very good approximation, this δy can be taken to be the same for all of the plane waves within the interferometer. Thus, the BB intensity for an interferometer with inserted wedge, illuminated by plane waves, is

$$I_{\mathrm{BB}}=\int_{-\infty}^{\infty} dy \left| \frac{\sin[(\pi t/\Delta)(y^2+1)^{1/2}]}{(y^2+1)^{1/2}} \right|^2 \times \left| \frac{\sin\{(\pi t/\Delta)[(-y+\delta y)^2+1]^{1/2}\}}{[(-y+\delta y)^2+1]^{1/2}} \right|^2 . \quad (10)$$

Note that reflection by the first crystal reverses the value of y for each wave approaching the second crystal, and that the limits on the integral are justified by the extremely sensitive relationship between y and θ_i and the fact that the reflectivity is negligible for large y values.

The parameter δy [which equals $\Delta/\pi t$ times ϕ_0, the parameter in Eq. (6a) describing the phase action of the wedge] is very small for any practical wedge. In this case, Eq. (10) can be shown to be essentially equivalent to Eq. (6a), which gives the BB central peak intensity for the wide-entrance-slit case. The square-root factors containing δy can be expanded, and with the help of trigonometric identities and a change of variables to $\Gamma=-y/(y^2+1)^{1/2}$, the integral of Eq. (10) can be transformed into that of Eq. (6a) plus some very rapidly oscillating sinusoidal terms. These extra terms in the full-plane-wave case can be interpreted as the interference in the second crystal of portions of each incident wave that would be blocked by an entrance slit. However, the contribution of these terms to the integral can be shown to be negligible when t/Δ is large.

It may seem surprising that Eq. (10) describes the effect of a wedge on the BB intensity for an interferometer with a wide entrance slit, because Eq. (10) has the form of a product of two intensities, and it is not easy to see how it describes the coherent splitting, spatial separation, and recombination of a neutron wave. The explanation is that splitting, separation, and recombination are all terms concerned with the *real-space* characteristics of the wave, while Eq. (10) is expressed in *wave-vector-space* language. (The variable y is related to the direction of propagation of the incident plane wave, and thus y determines the wave vector of the wave.)

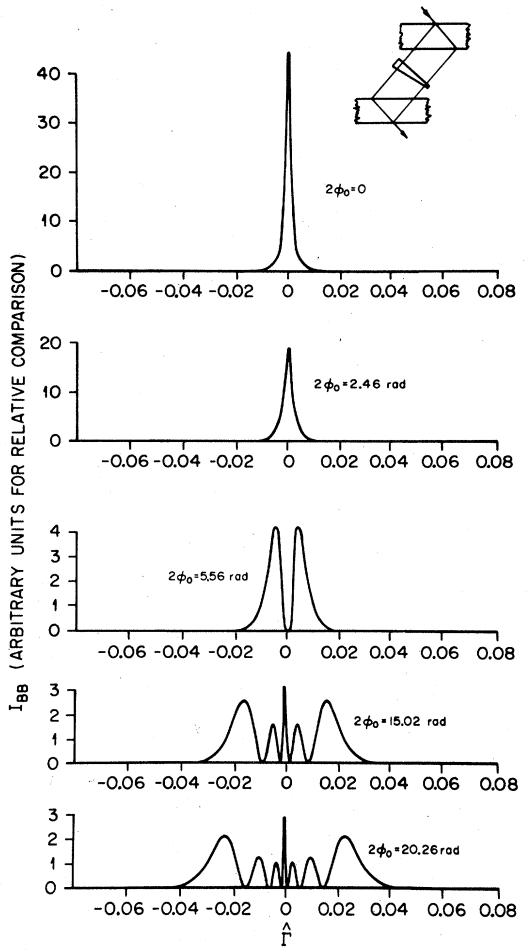

FIG. 5. Calculated intensity distribution in the BB beam as a function of phase wedge factor, for the case of a very narrow entrance slit.

It is not common practice to describe the operation of an interferometer in wave-vector space, but doing so leads to a useful relationship between the behavior of the interferometer with a wide entrance slit and with a very narrow one. Notice that Eq. (10), which gives the BB intensity in the wide-slit case, consists mathematically of the complete square integral of a function of y. Parseval's theorem states that this is equal to the complete square integral of the Fourier transform of this function. Now, there exists a Fourier-transform relationship

$$\frac{\sin[(\pi t/\Delta)(y^2+1)^{1/2}]}{(y^2+1)^{1/2}} \Longleftrightarrow \left[\frac{\pi t}{2\Delta}\right] J_0((\pi t/\Delta)(1-\Gamma^2)^{1/2})[\Theta(1-\Gamma)-\Theta(-1-\Gamma)] ,$$

where y and Γ are the conjugate variables.[17] The coordinate shift property of Fourier transforms gives another relationship:

$$\frac{\sin\{(\pi t/\Delta)[(-y+\delta y)^2+1]^{1/2}\}}{[(-y+\delta y)^2+1]^{1/2}} \Longleftrightarrow \left[\frac{\pi t}{2\Delta}\right] J_0((\pi t/\Delta)(1-\Gamma^2)^{1/2}) e^{i(\pi t/\Delta)\delta y\,\Gamma}[\Theta(1-\Gamma)-\Theta(-1-\Gamma)] .$$

Therefore, use of the Fourier convolution theorem along with Parseval's theorem implies that Eq. (10) is equivalent to

$$I_{\mathrm{BB}}=\mathrm{const}\times\int_{-2}^{2} d\hat{\Gamma} \left| \int_{\max(-1-\hat{\Gamma},\,-1)}^{\min(1-\hat{\Gamma},\,1)} d\Gamma\, J_0((\pi t/\Delta)[1-(\hat{\Gamma}+\Gamma)^2]^{1/2}) J_0((\pi t/\Delta)(1-\Gamma^2)^{1/2}) e^{i(\pi t/\Delta)\delta y\,\Gamma} \right|^2 . \quad (11)$$

Since $(\pi t/\Delta)\delta y = \phi_0$, this equation can be recognized as the total *integrated intensity* in the BB beam from an interferometer with a phase wedge and a very small entrance slit.

The conclusion is that despite significant differences between the coherence properties of the radiation inside an interferometer with a wide slit and one with a very narrow slit, and despite qualitatively different distributions of intensity in the exciting beams from a wide-slit interferometer with phase wedge and from one with a narrow slit, the functional dependence of the *total* BB intensity on a phase wedge is independent of the entrance-slit width. This result, which has also been reached via a different route by Bonse and Teworte,[18] has clear implications for anyone attempting to study experimentally the differences between wide-slit and narrow-slit interferometer behavior.

C. Narrow-slit experiments

From the above discussion, and from an examination of Fig. 5, it can be seen that in order to observe the effects of entrance-slit width on the operation of the interferometer, both a very narrow entrance slit and a very narrow exit slit must be used. In particular, these slits should have widths that are small compared to the *Pendellösung* length for the interferometer (84.1 μm for the MIT interferometer). Unfortunately, the available neutron flux at the MIT Research Reactor and the intrinsic low reflectivity of the perfect-silicon-crystal interferometer render impractical the use of slits less than about 100 μm wide. Therefore, it is necessary to consider the operation of the interferometer with slits of this intermediate size, in order to see if any of the narrow-slit behavior is discernible experimentally.

The use of an entrance slit whose width is finite is equivalent to placing a number of very narrow slits side by side. Thus, the wave amplitudes produced in an interferometer with an intermediate-sized entrance slit (on a *Pendellösung*-length scale) can be found by integrating narrow-slit wave amplitudes [Eq. (8)]. The coherence relationships between the points excited by a single plane wave must be observed in the integration. Also, since the beam incident on the entrance slit consists of a divergent mixture of plane waves, the intensities produced by the different incident plane waves must be added together. Notice that while the very-narrow-slit wave of Eq. (8) gives no information about the wave incident on the slit, the wave amplitude in the intermediate case does carry such information. Using the above procedure, the BB wave amplitude induced by a single plane wave, characterized by the parameter y, incident on an entrance slit of width α, can be written

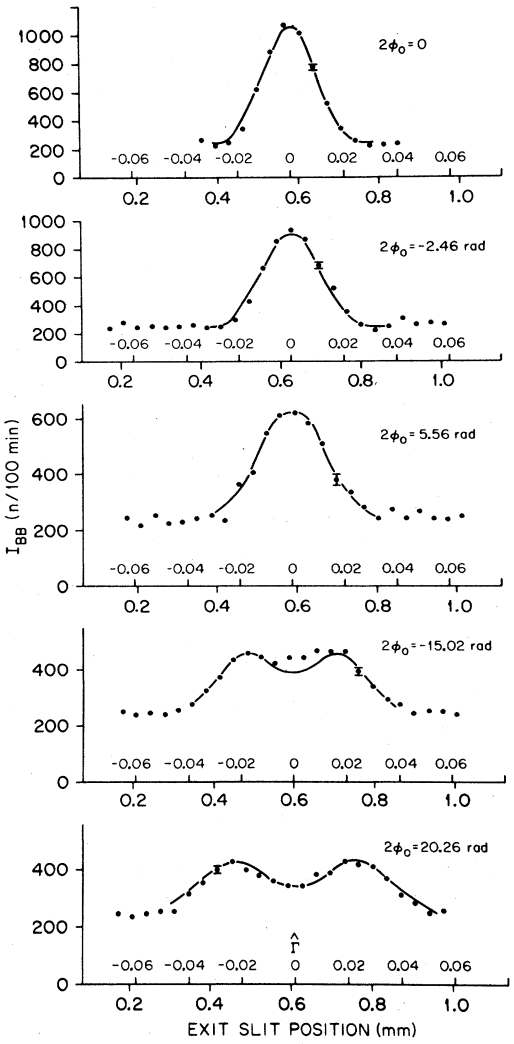

FIG. 6. Measured and predicted intensity distributions in the BB beam with various effective phase wedges, using entrance and exit slits of intermediate width ($\sim$0.1 mm).

$$\psi_{BB}(\hat{\Gamma},y) = \text{const} \times \int_{\hat{\Gamma}-\alpha/2t\tan\theta}^{\hat{\Gamma}+\alpha/2t\tan\theta} d\hat{\Gamma}'\, e^{i(\pi t/\Delta)y\hat{\Gamma}'} \times \int_{\max(-1-\hat{\Gamma}',\,-1)}^{\min(1-\hat{\Gamma}',\,1)} d\Gamma\, J_0((\pi t/\Delta)[1-(\hat{\Gamma}'+\Gamma)^2]^{1/2}) J_0((\pi t/\Delta)(1-\Gamma^2)^{1/2}) \,. \tag{12}$$

Note that $\hat{\Gamma}$ is defined with respect to a fixed point on the entrance surface of the first crystal. This point is taken to be at the center of the incident beam produced by the entrance slit. The dummy variable of integration $\hat{\Gamma}'$ is used to sum the contributions of waves from each entrance point allowed by the entrance slit. Finally, the BB intensity as a function of $\hat{\Gamma}$, for an interferometer which contains a phase wedge and has an entrance slit of width α illuminated by a divergent mixture of plane waves, is

$$I_{\mathrm{BB}}(\hat{\Gamma})=\text{const}\times\int_{-\infty}^{\infty}dy\left|\int_{\hat{\Gamma}-\alpha/2t\tan\theta}^{\hat{\Gamma}+\alpha/2t\tan\theta}d\hat{\Gamma}'\,e^{i(\pi t/\Delta)y\hat{\Gamma}'}\int_{\max(-1-\hat{\Gamma}',-1)}^{\min(1-\hat{\Gamma}',1)}d\Gamma\,J_0((\pi t/\Delta)[1-(\hat{\Gamma}'+\Gamma)^2]^{1/2})\times J_0((\pi t/\Delta)(1-\Gamma^2)^{1/2})e^{i\phi_0\Gamma}\right|^2. \tag{13}$$

In principle, the wavelength spread of the incident beam (which implies a spread of Δ values) should be accounted for; however, the 2.5% spread in the 1.564-Å monochromated beam used with the MIT interferometer has a negligible effect on the intensity distribution.

Figure 6 shows measured BB intensity distributions for several phase wedge values, using an entrance slit of width 115 μm (measured transversely to the incident beam) and an exit slit of width 96 μm. The solid curves are calculated numerically, based on Eq. (13) convoluted with the exit slit. The same background and intensity scaling factors have been used for all the curves, and the known variation in the interferometer's intrinsic wedge effect with beam height (which creates a small spread of effective wedge values around each of the values listed) has been included in the calculation. The agreement between experiment and calculation is excellent except for the $2\phi_0=-15.02$ rad case. The slight disagreement there may be due to physical defects in the wedge used. Though the structure in these intensity distributions is not as rich as would be expected if the slits were much narrower, some structure is definitely visible. It may also be noted that the integrated intensity, as a function of $2\phi_0$, is consistent with the wide-slit curve shown in Fig. 4. Thus, these experiments show the expected differences from the wide-slit behavior, and the expected similarities.

As a further demonstration of the effects of phase perturbations on the BB intensity distribution, a high-purity aluminum plate with a precisely machined step change in its thickness was inserted between the interferometer crystals so that the step was located at $\Gamma=0$. The height of the step, 0.290 mm, was chosen so as to change the relative phase of the neutron waves passing on either side of it by 3π radians. With the addition of this 3π phase step, the expected BB intensity distribution for the very-narrow-slit case is

$$I_{\mathrm{BB}}(\hat{\Gamma})=\text{const}\times\left|\int_{\max(-1-\hat{\Gamma},-1)}^{\min(1-\hat{\Gamma},1)}d\Gamma\,J_0((\pi t/\Delta)[1-(\hat{\Gamma}+\Gamma)^2]^{1/2})J_0((\pi t/\Delta)(1-\Gamma^2)^{1/2})e^{i\phi_0\Gamma}e^{3\pi i\Theta(\Gamma)}\right|^2. \tag{14}$$

The calculated distribution for the combination of a phase wedge specified by $2\phi_0=20.26$ rad and a 3π phase step is shown in Fig. 7(a).

For the finite slit, divergent beam case the BB intensity distribution is given by

$$I_{\mathrm{BB}}(\hat{\Gamma})=\text{const}\times\int_{-\infty}^{\infty}dy\left|\int_{\hat{\Gamma}-\alpha/2t\tan\theta}^{\hat{\Gamma}+\alpha/2t\tan\theta}d\hat{\Gamma}'\,e^{i(\pi t/\Delta)y\hat{\Gamma}'}\int_{\max(-1-\hat{\Gamma}',-1)}^{\min(1-\hat{\Gamma}',1)}d\Gamma\,J_0((\pi t/\Delta)[1-(\hat{\Gamma}'+\Gamma)^2]^{1/2})\times J_0((\pi t/\Delta)(1-\Gamma^2)^{1/2})e^{i\phi_0\Gamma}e^{3\pi i\Theta(\Gamma)}\right|^2. \tag{15}$$

Figure 7(b) shows the measured and calculated distributions using a 115-μm entrance slit and a 96-μm exit slit, for the $2\phi_0=20.26$ rad wedge and 3π phase step combination. The graphs shown in Fig. 7 should be compared with the corresponding graphs in Figs. 5 and 6 which depict the effects of a $2\phi_0=20.26$ rad wedge alone. That a localized discontinuity in the thickness of a transparent aluminum plate can cause such an overall change in the BB intensity distribution is a clear indication of the extended coherence of the neutron waves within the interferometer.

In performing these experiments using narrow slits, it was necessary to take into account a purely kinematical diffraction effect due to the divergence of the incident radiation. Because of the incident wavelength spread, divergence of the incident beam can propagate through the interferometer even though for any given wavelength the angular acceptance range of the perfect crystals is exceedingly small. However, it can be shown geometrically that the divergence effects should vanish at a distance behind the second interferometer crystal equal to the difference between the separation distance of the two crystals and the distance from the entrance slit to the first crystal. This geometrical focusing effect is illustrated in Fig. 8. Here, the exit slit was scanned across the very narrow central peak that arises when $2\phi_0=0$, for various positions of the entrance slit along the incident beam. The solid curve gives the predicted width of this peak using the known widths of the slits and the known divergence of the incident beam (0.0065 rad). The scans shown in Figs. 6 and

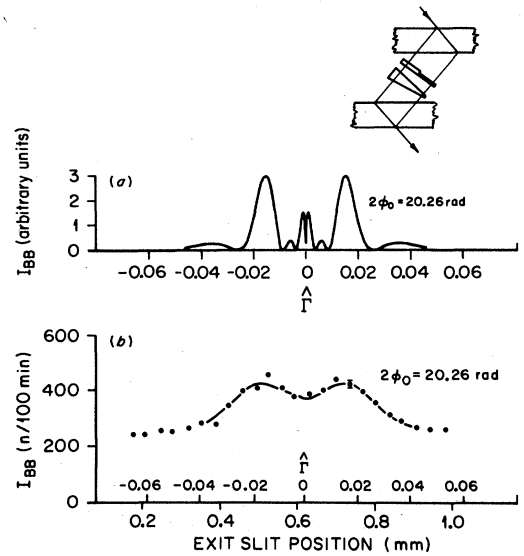

FIG. 7. (a) Calculated intensity distribution in the BB beam, for the very-narrow-slit case, using a $2\phi_0=20.26$ rad phase wedge and a centered 3π phase step plate. This graph should be compared with the corresponding graph in Fig. 5 which shows the effect of a 20.26-rad wedge alone. (b) Measured and predicted intensity distribution in the BB beam using slits of intermediate width (~ 0.1 mm), with a $2\phi_0=20.26$ rad phase wedge and a centered 3π phase step plate. Note that the peak positions differ from those of the graph in Fig. 6 which gives the distribution observed using the 20.26-rad wedge without the 3π step plate.

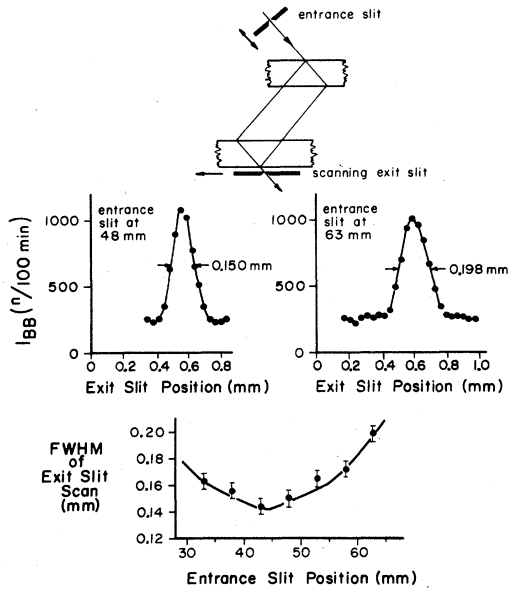

FIG. 8. Dispersive diffraction focusing of a divergent incident beam, measured by scanning the exit slit across the narrow central peak of the $2\phi_0=0$ intensity distribution (using 0.1-mm slits) for several positions of the entrance slit along the incident beam. Two representative scans are shown, along with a graph of measured and predicted peak width as a function of entrance-slit position.

7 were all performed with entrance and exit slits positioned to eliminate the effects of incident-beam divergence.

V. SUMMARY

An arrangement of thick perfect crystals such as the MIT two-crystal interferometer can be used to detect the effects of very weak perturbations of the phase of diffracting neutrons. The device also presents a challenge to the dynamical theory of neutron diffraction to explain the details of its operation. In this study attention has been directed at the manner in which the interferometer performance depends on the characteristics of the incident radiation. If this radiation is essentially of plane-wave character (that is, if the scale of its spatial structure is much larger than the *Pendellösung* length), then its spatial structure will not be modified by the diffraction process. This means that the operation of the interferometer with a wide (~ 1 mm) entrance slit can be analyzed using a ray optics approach, in which rays are coherently split by diffraction in the first crystal, follow separated paths between the crystals, and are partially recombined by diffraction in the second crystal. Such analysis has shown that the interferometer action manifests itself in the relative intensities of the BB and BF beams from a small focal region at the back of the second crystal. These beams each have about the same width as the entrance slit, and the intensity distribution within each beam does not exhibit any fine structure.

On the other hand, if the wave fronts of the incident radiation possess a certain amount of curvature, which can be induced by an entrance slit that is narrow compared to the *Pendellösung* length, then the dynamical diffraction process gives rise to a coherent spreading of the wave with a complicated *Pendellösung* structure. Tracking such a wave through the two crystals of the interferometer generally requires numerical evaluation of the integrals which arise. Such calculation has shown that interferometer action is present in very broad beams leaving the second crystal, though most of the intensity is concentrated in the middle parts of these beams. Both the intensities and the complicated spatial structure of these beams change when phase-shifting devices are inserted into the interferometer.

Connections between the wide-slit and narrow-slit interferometer behavior can be established through the Fourier-transform relationship between the diffracting wave excited in a crystal by a plane incident wave (expressed in wave-vector-space coordinates) and the wave excited by a very localized source wave (expressed in real-space coordinates). In particular, this relationship has been used to show that the form of the response to phase perturbations of the total integrated intensity of each of the beams leaving the interferometer is the same regardless of the width of the entrance slit. This fact implies that experiments designed to distinguish between wide-slit and narrow-slit behavior cannot simply measure the intensity of the exit beams, but rather must measure the distribution of this beam intensity.

Several such experiments have been performed. Using a wide (1 mm) entrance slit, the operation of the MIT in-

terferometer was in good agreement with the predictions of the ray optics analysis. Further experiments using narrow ($\sim$0.1 mm) entrance and exit slits were able to observe phase-shift-induced changes in the spatial intensity distribution in one of the exit beams, in excellent agreement with calculations based on dynamical diffraction theory. Unfortunately, intensity limitations did not permit the use of very narrow ($\sim$0.01 mm) slits, which would be expected to reveal much more dramatic intensity distribution effects. It is conceivable that very-narrow-slit interferometer experiments would be possible at a high-flux reactor.

The very good agreement between the experiments described here and the dynamical diffraction theory serves to reaffirm the validity of the wave-mechanical theory of matter. In passing through the interferometer, the neutron wave function is coherently spread over quite macroscopic distances—an extremely nonclassical situation. By making such nonclassical concepts operationally accessible, neutron interferometry offers a unique testing ground for the principles of quantum mechanics.

ACKNOWLEDGMENTS

The authors wish to thank Professor M. A. Horne and Dr. D. K. Atwood for helpful discussions, and Mr. Armand D'Addario for invaluable assistance in fabricating the interferometer and the various devices used in the present study. This research was supported by National Science Foundation Grant No. DMR-80-21057-A02.

---

*Present address: Solid State Division, Oak Ridge National Laboratory, Oak Ridge, TN 37831.

†Permanent address: Atominstitut der Österreichischen Universitäten, A-1020 Wien, Austria.

[1]D. Sippel, K. Kleinstück, and G. E. R. Schulze, Phys. Lett. **14**, 174 (1965).

[2]C. G. Shull, Phys. Rev. Lett. **21**, 1585 (1968); C. G. Shull and J. A. Oberteuffer, *ibid.* **29**, 871 (1972).

[3]H. Rauch, W. Treimer, and U. Bonse, Phys. Lett. **47A**, 425 (1978).

[4]A. Zeilinger, C. G. Shull, J. Arthur, and M. A. Horne, Phys. Rev. A **28**, 487 (1983).

[5]H. Rauch and D. Petrascheck, in *Neutron Diffraction,* edited by H. Dachs (Springer, Berlin, 1978).

[6]U. Bonse and W. Graeff, in *X-Ray Optics,* edited by H.-J. Queisser (Springer, Berlin, 1977).

[7]J. Arthur and M. A. Horne, preceding paper [Phys. Rev. B **32**, 5747 (1985)].

[8]N. Kato, in *X-Ray Diffraction,* edited by L. Azaroff (McGraw-Hill, New York, 1979).

[9]V. L. Indenbom and F. N. Chukhovskii, Usp. Fiz. Nauk **107**, 229 (1972) [Sov. Phys.—Usp. **15**, 298 (1972)].

[10]A. Zeilinger, C. G. Shull, M. A. Horne, and G. L. Squires, in *Neutron Interferometry,* edited by U. Bonse and H. Rauch (Oxford University Press, New York, 1980).

[11]S. Kikuta, in *Neutron Interferometry,* edited by U. Bonse and H. Rauch (Oxford University Press, New York, 1980).

[12]D. K. Atwood, Ph.D. thesis, Massachusetts Institute of Technology, 1982 (unpublished); J. Arthur, Ph.D. thesis, Massachusetts Institute of Technology, 1983 (unpublished); C. G. Shull, in *Physics as Natural Philosophy,* edited by A. Shimony and H. Feshbach (MIT Press, Cambridge, 1982).

[13]C. G. Shull, D. K. Atwood, J. Arthur, and M. A. Horne, Phys. Rev. Lett. **44**, 765 (1980).

[14]D. M. Greenberger, D. K. Atwood, J. Arthur, C. G. Shull, and M. Schlenker, Phys. Rev. Lett. **47**, 751 (1981).

[15]D. K. Atwood, M. A. Horne, C. G. Shull, and J. Arthur, Phys. Rev. Lett. **52**, 1673 (1984); **53**, 1300(E) (1984).

[16]U. Bonse, W. Graeff, and H. Rauch, Phys. Lett. **69A**, 420 (1979).

[17]The fact that the wave function excited in a crystal by a plane incident wave and the wave function excited by a spatially very limited wave are Fourier transforms is not simply accidental—see Ref. 7.

[18]U. Bonse and R. Teworte, Z. Naturforsch. **37a**, 427 (1982).

[19]The plane-wave approach has been considered in detail by D. Petrascheck and H. Rauch, Acta Crystall. A **40**, 445 (1984).